doi.org/10.15407/tpwj2017.07.02

STRUCTURE AND SERVICE PROPERTIES OF WELDED JOINTS OF HIGH-STRENGTH STEELS, ALUMINIUM AND TITANIUM ALLOYS

L.I. MARKASHOVA, V.D. POZNYAKOV, E.N. BERDNIKOVA, T.A. ALEKSEENKO, O.S. KUSHNAREVA and **E.V. POLOVETSKY**
E.O. Paton Electric Welding Institute, NASU
11 Kazimir Malevich Str., 03680, Kiev, Ukraine. E-mail: office@paton.kiev.ua

A structural-analytical approach to evaluation of effect of structural-phase states on change of the most significant mechanical properties of examined materials was used in this work. A role of structural factors (alloying type, phase composition, size of grain and subgrain structure, distribution and density of dislocation, phase precipitations, their size and nature of distribution) was shown for ensuring optimum properties of welded joints and their operation reliability. Experimental-analytical evaluations have determined structural-phase parameters and factors providing the necessary complex of welded joint properties. 20 Ref., 2 Tables, 12 Figures.

Keywords: *argon-arc welding, friction stir welding, electron beam welding, hybrid laser-arc welding, aluminium alloy, heat-resistant titanium alloy, high-strength steel, welded joints, structure, phase composition, mechanical properties, fracture toughness, crack resistance*

Welded joints of complexly-alloyed aluminium and titanium alloys, high-strength and heat-resistant steels, produced by different welding methods (fusion, pressure) and widely used in aircraft and aerospace engineering, machine building and manufacture of critical designation structures require necessary mechanical properties. The latter are determined by structural-phase state of metal in a welding zone [1–5]. At that such welding methods (fusion, pressure) are selected, which could provide high process productivity as well as necessary complex of service properties of welded joints, namely indices of strength, ductility and crack resistance.

In this context it is very relevant to consider the issue of structure effect on properties of the welded joints of such materials as high-strength steels, complexly-alloyed aluminium as well as titanium alloys. The latter in course of technological processes of welding are characterized with dramatic change of phase composition, structure parameters, phase precipitations (PP) etc. At that there is a general understanding of the problem, however no clear vision, which structural-phase factors and parameters of the forming structures effect improvement of mechanical properties and crack resistance of welded joints that outline specific problems for investigation of these problems.

Solution of these problems requires, first of all, examination of structural state of metal of welded joints at all structural levels, including optical metallography, scanning and transmission electron microscopy. As for structural-phase states, then such a complex should include the most noticeable for service properties structural indices, i.e. phase composition, content of alloying elements, size of grain and subgrain structure, phase formations (their composition, size and distribution), and, what is very important, nature of dislocation density distribution. A complex analysis of structural-phase state allows carrying out analytical evaluation of specific input of all structural-phase parameters in main service properties of the welded joints, namely strength, ductility and crack resistance.

Therefore, aim of the present work from point of view of interconnection of welding modes → structure → joint properties lies in investigation of a role of structure and phase composition of the welded joints of specific materials (high-strength steels, complexly-alloyed aluminium and titanium alloys), produced by different welding methods (hybrid laser-arc welding, argon-arc welding, friction stir welding, electron beam welding) on change of service properties, i.e. strength, ductility and crack resistance of welded joints.

Materials and investigation procedures. The work was performed on the specimens of high-strength steel 14KhGN2MDAFB (0.183 % C, 1.19 % Cr, 0.98 % Mn; 2.07 % Ni; 0.22 % Mo; 0.08 % V; 0.33 % Si, not more than 0.018 % P and 0.005 % S) of up to 10 mm thickness using welding wire Sv-10KhN2GSMFTYu (≤0.1 % C; 0.7 % Cr; 0.4 % Mn; 0.22 % Mo; 0.15 % V; 0.24 % Si; not more than 0.007 % S) at the following modes of laser-arc welding, namely 1st mode — v_w = 72 m/h, I ~ 125 A,

U_a ~ 23V; 2nd mode — v_w = 90 m/h, I ~ 150 A, U_a ~ ~ 25V; 3rd mode — v_w = 110 m/h, I ~ 200 A, U_a ~ ~ 26 V. Indicated modes allow providing cooling of HAZ metal in 600–500 °C interval range with $w_{6/5} \approx$ ≈ 58–62 °C/s rate. Laser radiation power source was Nd:YAG-laser DY 044 (Rofin Synar, Germany) of up to 4.4 kW radiation power and shielding gas (mixture of Ar + CO_2 with 15–20 l/min consumption) [6].

Welded joints of complexly-alloyed Al–Li alloys 1460 (wt.%): 0.1 Si; 0.15 Fe; 3.0 Cu; 0.1 Mn; 0.1 Mg; 0.05 Cr; 0.25 Zn; 0.04 Ti; 0.1 Zr; 2.3 Li; 0.09 Sc; 0.008–0.1 Be were produced using argon-arc non-consumable electrode welding (AANEW) on MW-450 machine (Fronius, Austria) under the following conditions: rate 20 m/h and current 140 A using filler materials Sv1201 and Sv1201 + 0.5 % Sc. In parallel structural-phase states of the welded joints, made by friction stir welding (FSW) without filler material on laboratory unit designed at the E.O. Paton Electric Welding Institute, were investigated. In the latter case, butt joints were made using special tool with cone pin and shoulder 12 mm diameter, at that rotation rate of the tool made 1420 rpm and linear rate of its movement along the joint was 14 m/h [7].

Interconnection of composition → structure → properties was evaluated by investigation of the welded joints of two pilot heat-resistant multicomponent titanium alloys, made by electron beam welding (EBW) depending on silicon alloying. Both alloys contain silicon as an alloying element and refer to pseudo α- (alloy 1) and α + β (alloy 2) titanium alloys (Table 1) [8].

The structural-phase characteristics, i.e. size of grain and subgrain structure, distribution of phase precipitations, peculiarities of zones of brittle and tough fracture, nature of dislocation density distribution in weld metal and different areas of HAZ of welded joints were examined at all structural levels using a complex of experimental methods of modern physical metal science, including optical metallography (microscopes «Versamet-2» and «Neophot-32»), analytical scanning microscopy (SEM-515, Philips company) and transmission electron microscopy (JEM-200CX, JEOL Company). Hardness of examined metal was measured on M-400 microhardness tester of LECO Company.

Analytical evaluation of welded joint service properties. Complex investigations carried at all structural levels (from grain to dislocation) allowed evaluating differential input of various structural-phase constituents and their parameters (grain size D_g, subgrain d_s, sizes of d_{pp} and distribution of PP particles, dislocation density ρ, inter particle distance λ_p, volume fraction of forming structures) in change of mechanical properties σ_y, fracture toughness K_{1c} as well as local internal stresses ($\tau_{l/in}$ — zones of nucleation and propagation of cracks) in different areas of the welded joints with used technological modes of welding [6–16].

Table 1. Composition of pilot heat-resistant titanium alloys, wt.%

Alloy	Al	Sn	Zr	Mo	V	Nb	Si
1	5.2	3.3	4.2	0.1	0.6	0.8	0.6
2	4.3	4.4	6.0	1.6	0.7	4.3	0.4

Mechanical properties. Integral values of hardening ($\Sigma\sigma_h$) were evaluated (according to equation including known dependencies of Hall–Petch, Orowan etc. [11–15]) as a sum value consisting of series of constituents: $\Sigma\sigma_y = \Delta\sigma_0 + \Delta\sigma_{s.s} + \Delta\sigma_g + \Delta\sigma_s + \Delta\sigma_d + + \Delta\sigma_{disp.hard}$, where $\Delta\sigma_0$ is the resistance of type of metal lattice to movement of free dislocations (stress of lattice friction or Peierls–Nabarro stress); $\Delta\sigma_{s.s}$ is the hardening of solid solution with alloying elements, according to Mott–Nabarro theory; $\Delta\sigma_g$ and $\Delta\sigma_s$ are hardening due to change of grain and subgrain in accordance with Hall–Petch dependence; $\Delta\sigma_d$ is the dislocation hardening, caused by interdislocation interaction on J. Taylor, A. Zeger, N. Mott and G. Hirsch theory as well as $\Delta\sigma_{disp.hard}$ is the dispersion hardening due to dispersion phases by Orowan.

Fracture toughness. Calculation values of fracture toughness indices K_{1c} are evaluated on dependence [17]: $K_{1c} = (2E\sigma_y\delta_c)^{1/2}$, where E is the Young's modulus; σ_y is the calculation value of hardening; δ_c is the value of critical crack opening (according to data of substructure parameters).

Crack resistance (local and internal stresses). Analysis of different approaches to mechanisms of crack nucleation and fracture of materials was used for selection of an evaluation based on dislocation theory of crystalline solid bodies considering analysis of nature of dislocation structure and its distribution (dislocation accumulations or uniform dislocation distribution). This allows carrying detailed evaluation of a level of dislocation internal stresses depending on zones of dislocation accumulations, namely along sub- or intergranular boundaries, in PP zones and their accumulations etc, which promote formation of concentrators of local internal stresses, i.e. zones of nucleation and propagations of cracks. A field of internal stresses, developed by dislocation structure (dislocation density) is described by expression [18–20] $\tau_{in} = = Gbh\rho/[\pi(1 - \nu)]$, where G is the shear modulus; b is the Burgers vector; h is the foil thickness, v is the Poisson's ratio; ρ is the dislocation density.

Results of experiment. The welded joints of high-strength steel produced by hybrid laser-arc and arc welding [6] were investigated. Complex investigations at all structural levels determined changes of different phase constituents (upper bainite B_u and lower B_l, martensite M), their volume fraction v_f, %,

Table 2. Change of volume fraction (v_f, %) of phase constituents (B_l, B_u, M), grain value (D_g) and integral microhardness (*HV*) in welded joints at different rates of welding

Indices/Area	v_w = 72 m/h		v_w = 90 m/h		v_w = 110 m/h	
	Weld	HAZ	Weld	HAZ	Weld	HAZ
v_f, % / Parameters	B_l ~ 60 % B_u ~ 20 % M ~ 20 %	B_l ~ 80 % B_u ~ 5 % M ~ 15 %	B_l ~ 20 % B_u ~ 15 % M ~ 65 %	B_l ~ 30 % B_u ~ 20 % M ~ 50 %	B_l ~ 10 % B_u ~ 60 % M ~ 30 %	B_l ~ 20 % B_u ~ 70 % M ~ 10 %
D_g, μm	30–120×170–350	30–60	30–80×150–300	25–50	20–80×150–250	20–40
HV, MPa	3800–4010	3540–3900	4050–4420	3830–4010	3360–3940	3360–4010

microhardness (*HV*) as well as different structural parameters (values of grain and subgrain structures D_g, d_s), typical distributions and dislocation densities (ρ) as well as peculiarities of fracture zone of welded joints (tough, brittle etc.) depending on used rates of laser-arc welding (v_w = 72; 90; 110 m/h).

It is shown that v_w = 72m/h promotes formation of mainly B_l structure in weld metal and HAZ of welded joints, and at transfer from weld to HAZ metal the grain structure significantly refines (2–4 times) at uniform decrease (per 12 %) of microhardness, Table 2. Increase of welding rate (v_w) from 72 to 90 m/h provides variation of phase composition of weld metal and HAZ of the welded joints from bainite-martensite (B–M) to martensite (M) type as well as relationship of structural constituents in HAZ metal of the welded joints: volume fraction of B_l decreases 2–3 times at 3 times rise of fraction of M_{temp}. This, as a result, provides the maximum indices of strength, however, leads to substantial decrease of ductility ψ in the weld. In the case of increase of welding rate to v_w = 110 m/h, regardless the fact that phase composition of weld metal and HAZ overheating area are the same as at v_w = 72 m/h modes, i.e. bainite-martensite, the maximum v_w provokes significant volume fraction of B_l to 10–20 % and formation of mainly B_u structure (60–70 %). Such structural changes can result in non-uniform level of mechanical properties along the welding zone and decrease of crack resistance of welded joints.

Detailed electron microscopy transmission investigations of structures of the welded joints, made at v_w = 72 and 110 m/h, determined the following.

Formation of inner substructure with uniform distribution of volume dislocation density (ρ) up to (4–6)·10^{10} cm^{-2} is observed in B_l grains of weld metal, at v_w = 72 m/h and in M_{temp} structures dislocation density makes 8·10^{10}–10^{11} cm^{-2}. Fragmentation of B_l grains is typical for HAZ metal of the joints, i.e. 10–20 % refinement of lath structure of B_l and M_{temp} is observed. It is accompanied by somewhat increase of dislocation density (Figure 1, *a*).

The following is typical for fine metal structure of welded joint in the case of v_w = 110 m/h, i.e. integral value of dislocation density in weld metal and HAZ rises, mainly upper bainite B_u structure is formed at maximum increase of dislocation density ρ to 1.5·10^{11} cm^{-2} (see Figure 1, *b*).

Thus, it is shown that the most uniform distribution of dislocation density in formation of lower bainite structure B_l is provided at hybrid laser-arc welding mode with v_w = 72m/h rate.

The following was determined as a result of carried evaluations on changes along the welding zone of such strength characteristic as σ_y. Calculation value $\Sigma\sigma_y$ makes 917 and 1077 MPa, respectively, in weld metal and HAZ under conditions of v_w = 72 m/h, and the maximum input in yield strength has substructural ($\Delta\sigma_s$ ~ 318–356 MPa), dispersion ($\Delta\sigma_{disp.hard}$ ~ 253–295 MPa) and dislocation ($\Delta\sigma_d$ ~ 157–180 MPa) hardening (Figure 2, *a*). At that input of such type of structural constituent as lower bainite (B_l) is the maximum one (Figure 2, *b*).

In the case of welding modes at v_w =110 m/h the total value of yield strength rises (in comparison with v_w = 72 m/h mode) by 10–15 % (Figure 3) that is caused by somewhat refinement of grain structure and

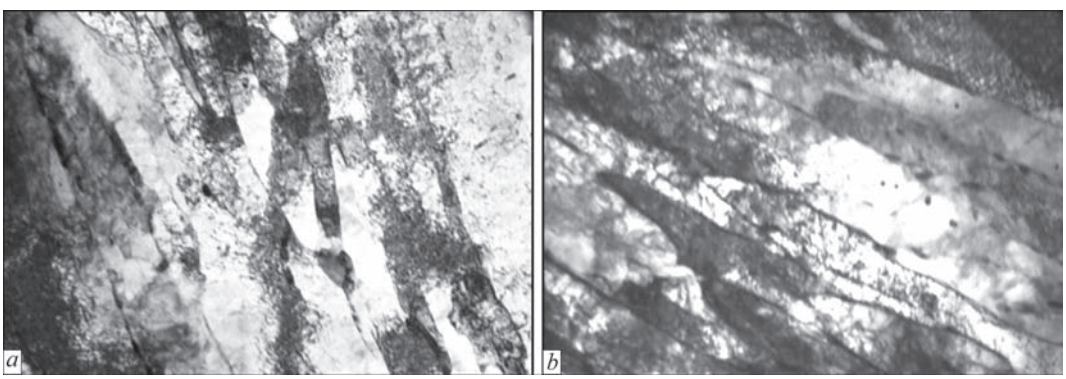

Figure 1. Fine structure of HAZ metal: *a* — lower bainite at v_w = 72 m/h (×20000); *b* — upper bainite (×30000) at v_w = 110 m/h

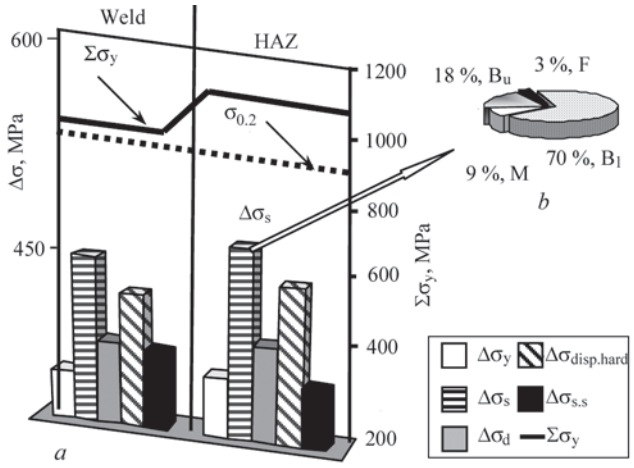

Figure 2. Input of different constituents Δσ of structural hardening in calculation value of yield limit $\Delta\sigma_y$ of weld metal (*a*) and input of structural constituents (B_u, B_l, M_{temp}, F) in change of substructural hardening $\Delta\sigma_s$ at welding rate 72 m/h (*b*)

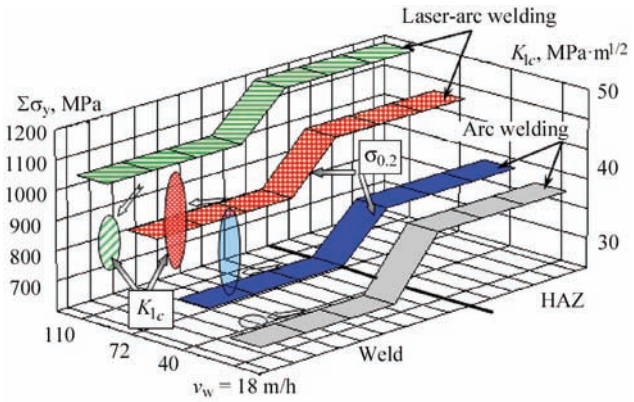

Figure 3. Change of average calculation value of yield limit ($\Sigma\sigma_y$) and fracture toughness (K_{1c}) along welding zone (weld, HAZ) of steel 14KhGN2MDAFB at different rates of hybrid laser-arc (v_w = = 72 m/h and 110 m/h) and arc (v_w = 18 m/h and 40 m/h) welding

increase (1.3 times) of integral value of dislocation density (ρ).

The following is shown by the calculation values of fracture toughness indices K_{1c} as well as comparison of K_{1c} and σ_y (see Figure 3). If with v_w = 72 m/h the substructure, which is mainly lower bainite (B_l) substructure, makes the largest input in metal hardening ($\Sigma\sigma_y$) and increase of fracture toughness (K_{1c}), then in the case of increased welding rate v_w = 110 m/h K_{1c} index significantly decreases (30 %). The latter is caused by dominating formation of another type of structure, namely upper bainite (B_u) with corresponding further nonuniform distribution of dislocation density (ρ).

Further comparative analysis of calculation indices of strength properties (σ_y) and fracture toughness (K_{1c}) for the investigated welded joints of high-strength steel 14KhGN2MDAFB, produced using different modes of welding (arc welding and hybrid laser-arc one), showed that the best indices combining properties of strength and toughness are provided by modes of hybrid welding (see Figure 3).

The results of evaluation of change in the level of local internal stresses showed that the maximum values of $\tau_{l/in}$ ~ 1900–2800 MPa ((0.2–0.35)τ_{theor} from theoretical strength) are formed at v_w =110 m/h in the places of extended dislocation accumulations ($\rho = 1.5\cdot10^{11}$ cm^{-2}) along B_u boundary. This results in nucleation of microcracks in these zones and decrease of crack resistance of welded joints (Figure 4, *a*, *b*). And the lowest values of τ_{in} (around 1500–1800 MPa) are typical for welded joints received at v_w = 72 m/h. It is promoted by formation in the welding zone of fine grain and fragmented B_l structures in combination with uniform distribution of dislocations (Figure 4, *c*, *d*).

It is determined as a result that the optimum properties of strength, ductility and crack resistance of high-strength steel welded joints are provided under conditions of v_w = 72 m/h welding rates. It is caused by formation of the most dispersed structures, namely lower bainite, fine grain martensite tempered in ab-

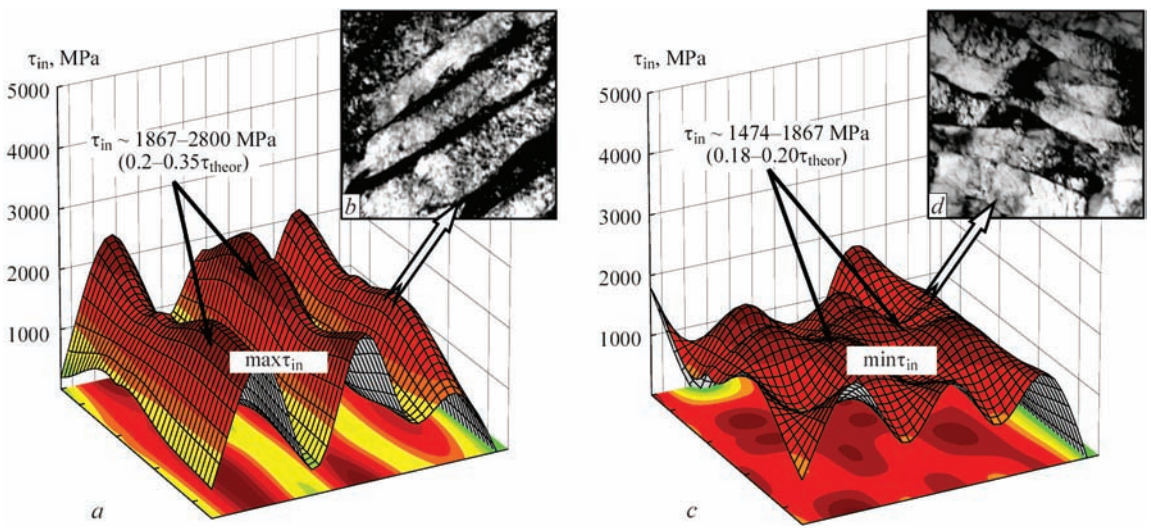

Figure 4. Distribution of local internal stresses (τ_{in}) in weld metal in structural zones of upper bainite at v_w = 110 m/h (*a*, *b*, ×20000) and lower bainite at v_w = 72 m/h (*c*, *d*, ×30000)

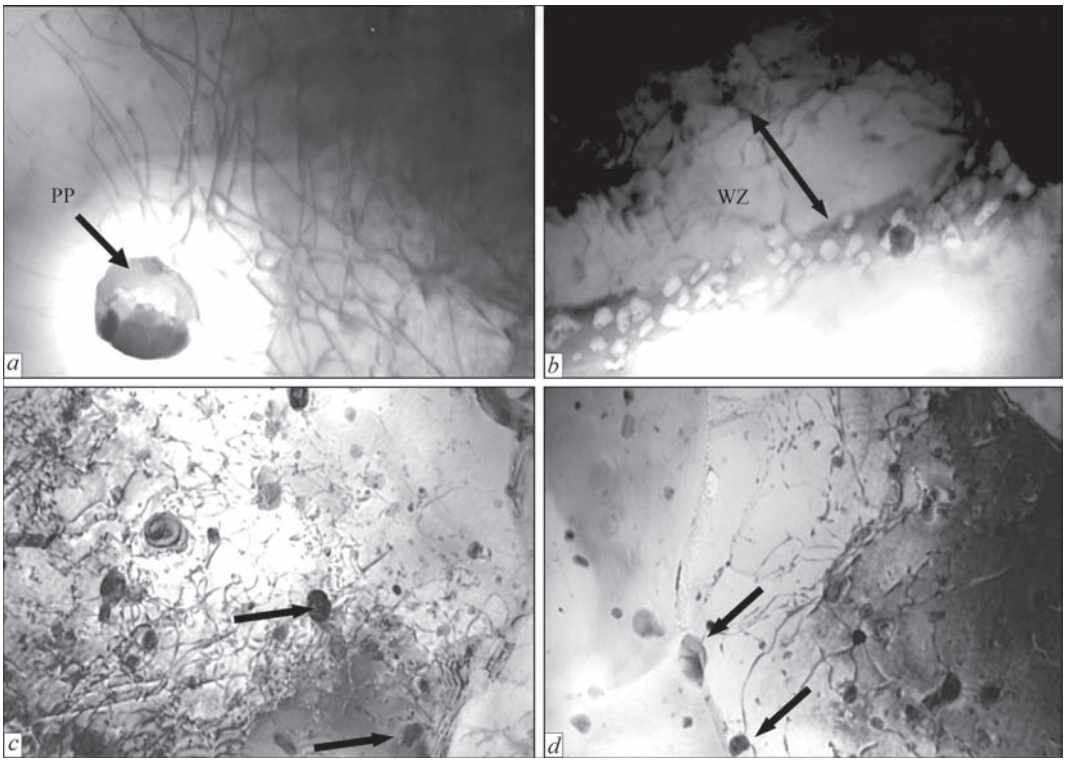

Figure 5. Distribution of phases in grain volumes of weld metal of aluminium alloy 1460 produced by AANEW: *a* — phase precipitations in internal grain volumes; *b* — near-boundary zones free from precipitations and FSW: *c* — phase precipitations in grain volumes; *d* — phase precipitations in grain boundary zones of weld metal (×30000)

sence of extended dislocation accumulations — concentrators of local internal stresses ($\tau_{l/in}$).

Welded joints of complexly-alloyed aluminium-lithium alloys (argon-arc welding and FSW) [7]. The following is determined as a result of investigation of welded joints of aluminium alloys, produced by AANEW without and with scandium alloying. Weld metal of the welded joints of Al–Li alloy 1460 using filler material Sv1201 (without scandium alloying) after AANEW is characterized with coarse grain structures; formation of large globular intergranular phase precipitations (d_{pp} size up to 3.5 μm, Figure 5, *a*), extended massive intergranular eutectics (thickness h_{eut} to 5 μm and zones free from precipitations (ZFP) (Figure 5, *b*).

At that, non-uniformity of dislocation distribution is noted, in particular along the extended near-boundary zones, where dislocation density ρ drops virtually by order in comparison with intergranular dislocation density from $\rho \sim (2–6)\cdot10^9$ cm^{-2} (Figure 5, *a*, *b*).

Scandium alloying of weld metal (up to 0.5 %) promotes the following changes in structure of welding zone metal, i.e. refinement of grain structure, grain boundary eutectics, dispersion of phase precipitations in grain volumes in combination with somewhat increase of dislocation density to $\rho \sim (4–9)\cdot10^9$ cm^{-2}.

Investigations of peculiarities of structural changes in FSW determined significant structure refinement; increase of total dislocation density to $\rho \sim (3–6)\cdot10^{10}$ cm^{-2} (that is an order higher than the dislocation density of weld metal in fusion welding, Figure 5, *a*, *b*) accompanied by active redistribution of dislocations and formation of substructure (blocks, fragments, etc.); substantial refinement (2.5–5.0 times) of PP at increase of their volume fraction and uniform distribution along intergranular as well as grain boundary volumes (Figure 5, *c*, *d*).

The results of the analytical evaluations of mechanical properties ($\Sigma\sigma_y$) of investigated joints after AANEW with scandium and without it showed the highest indices in scandium alloyed joints (Figure 6).

At that, the largest input in total (integral) value of hardening of weld metal with scandium has grain ($\Delta\sigma_g \sim 29$ %) and solid solution ($\Delta_{s.s} \sim 25$ %) hardening. Under FSW conditions the evaluations of total (integral) values of $\Sigma\sigma_y$ showed the total increase of values of strength indices by 40 % in comparison with such for AANEW welding conditions without scandium. It is provided mainly by refinement of grain (to 27 %) and subgrain (to 21 %) structures and PP dispersion (to 23 %).

Comparison of properties of fracture toughness (K_{1c}) of the investigated joints showed the following. After AANEW without scandium toughness index is $K_{1c} \sim 26–47$ MPa·m$^{-1/2}$ (Figure 7, *a*, *b*). As a result of FSW application K_{1c} is preserved at the level of $K_{1c} \sim 31–57$ MPa·m$^{-1/2}$ (Figure 7, *a*, *c*) that indicates increase (by 20 %) of ductility properties of welded

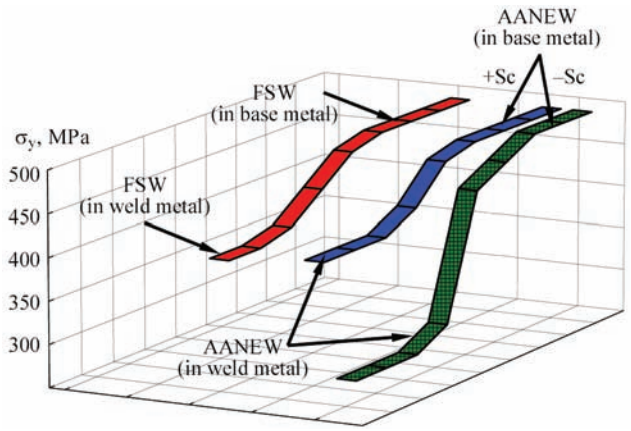

Figure 6. Change of integral value of hardening $\Sigma\sigma_y$ of welded joints of aluminium alloy 1460 at transfer from base metal to weld metal produced by AANEW using filler materials Sv1201 and Sv1202 + 0.5 % Sc, and FSW

joint in comparison with conditions of AANEW without scandium.

Specific results of the investigations and, first of all, nature of dislocation structure distribution in the investigated specimens allowed evaluating local internal stresses ($\tau_{l/in}$), determine their level and extension as well as determine structural factors provoking processes of crack nucleation and propagation.

The analytical evaluations determined, as a result, that the extended concentrators of local internal stresses with $\tau_{l/in}$ level to 1500 MPa (from 0.34 to $0.85\tau_{theor}$) are formed under AANEW conditions in metal without scandium. These are the zones of crack nucleation and propagation. The boundaries of strong shear bands (SB) (Figure 8, *a*, *b*) refer to such zones. In contrast to this, values of $\tau_{l/in}$ rapidly decrease (virtually two orders) to value approximately 5–15 MPa ($0.0016–0.0055\tau_{theor}$) in the internal volumes of SB. This, as a result, develops a strong gradient ($\Delta\tau_{l/in}$) of local internal stresses along SB boundaries (Figure 8, *b*).

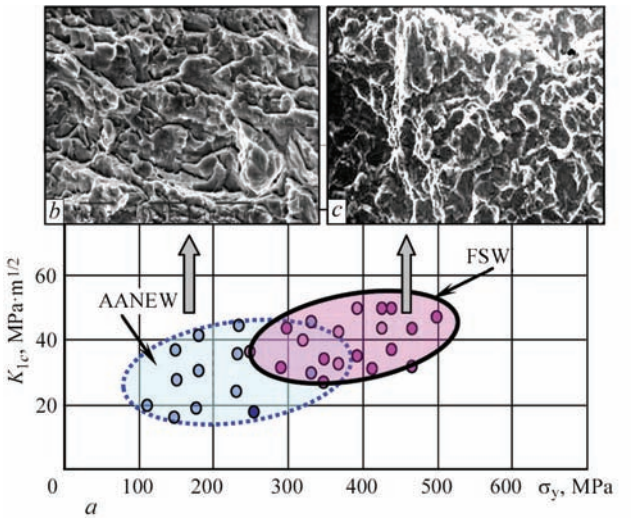

Figure 7. Change of calculation values of strength $\Sigma\sigma_y$ and fracture toughness K_{1c} of weld metal (*a*) and fractograms (×2020): *b* — brittle fracture of aluminium alloy 1460 produced by AANEW using filler material Sv1201; *c* — tough fracture at FSW

Microstructure of the weld metal under FSW conditions represents general significant decrease (3.5 times) of the level of local internal stresses (to 221–447 MPa) at uniform (without gradients) distribution of such type of local stresses along the whole volume of weld metal (Figure 8, *c*, *d*) that provides rise of welded joint crack resistance.

Thus, improvement of strength characteristics and crack resistance of the welded joints of complexly-alloyed aluminium alloys requires aiming at formation of the optimum structure that is provided by FSW as shown by investigations of structure and properties interconnection.

Welded joint of titanium alloys (electron beam welding) [8]. Metallographic examinations of structure of the most problematic zone of welded joints, namely heat-affected zone (HAZ), determined that

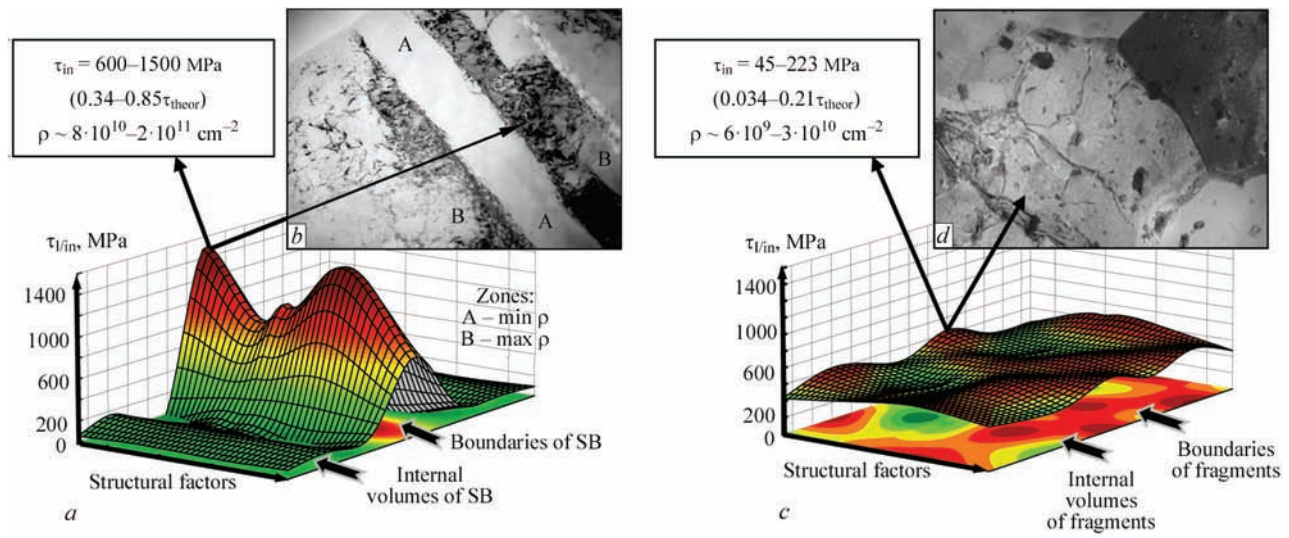

Figure 8. Distribution of local internal stresses $\tau_{l/in}$ in weld metal of alloy 1460 after different welding methods: *a*, *b* — AANEW (weld metal without scandium); *c*, *d* — FSW

formation of cold cracks of 100–300 μm length is observed after welding in a near-weld zone (NWZ). Moreover, volume fraction of cracks is significantly higher in the welded joints of pilot alloy 1, than in the welded joints of alloy 2. At that, the NWZ of welded joint of pilot alloy 1 in cooling contains the coarse equiaxial polyhedral primary β-grains of up to 500 μm size. The NWZ of welded joints of alloy 2 has a nonuniform primary structure. Together with the vast areas of polyhedral grains of 200 μm size there are areas of fine equiaxial grains of 20–60 μm size in the coarse grain surrounding. Intergranular structure in the NWZ of alloy 1 and NWZ of alloy 2 is martensite α′-phase characterized with fine acicular structure. Residual β-phase can be present in the NWZ of both alloys in addition to martensite phase. Its amount in alloy 1 following from composition is very small, and it is more in alloy 2, than in alloy 1. More detailed structural-phase investigations of HAZ of welded joints of titanium alloys were carried out using scanning microdiffraction electron microscopy for determination of composition of the forming phases as well as their size, morphology and structural zones of their localizing.

The results of examination of dislocation structure and processes of phase formation showed essential difference in the structural-phase state of α′- and β lamellar structures in the welded joints of pilot alloy 1. Parallel formation of dramatically different on structural-phase composition lamellar structures takes place, namely virtually dislocation-free ($\rho \sim 10^9 \cdot cm^{-2}$) and containing no phase precipitations of the lamellas of extended shape (with cross-section $h_{lam} \sim 0.3–1.6$ μm, Figure 9, *a*) together with the lamellas characterized with high dislocation density (to $\rho \sim (7–8) \cdot 10^{10}$ cm^{-2}) and saturation of inner lamella volumes with chaotically distributed precipitations, mainly Ti_5Si_3 of sufficiently coarse size ($d_{pp} \sim 0.1–0.2$ μm, Figure 9, *b*) and dispersed PP (Ti_2ZrSi_3; Ti_3Al) fringing the interlamellar structure. Formation of the strong gradient (on phase precipitations and dislocation density) lamellas is caused, apparently, by type of crystalline lattice, corresponding to β- and α-formations in titanium alloys. Thus, for β-phase having BCC-lattice (this is up to 48 slip systems) there is virtually unlimited possibility of nucleation, slip and redistribution of the dislocations, which, as it is well known, are active channels for transporting alloying elements and, respectively, activation of phase formation processes. The α-structure, having HCP-lattice, is characterized with very limited amount of the slip systems. Mainly, it is one base (0001) plane and deformation in a metal with such type of lattice is mostly realized due to twinning, when nucleation and dislocation slip is virtually complicated, so that as phase formation.

Apparently, different peculiarities of processes of deformation realizing (dislocation slip or twinning) and as a result different possibilities of phase formation for main phase constituents (α- and β-phases) are the explanation of formation of strong gradient on dislocation density and saturation by phase precipitations of the extended lamellar structures in the welded joint of pilot alloy 1.

Thus, it is determined that presence of gradient structural-phase formations, significantly different on amount and dispersion of silicide phases, including on dislocation density, is apparently the basis for formation in metal of such type of corresponding strong gradient mechanical characteristics, namely, gradients on strength properties ($\sigma_{0.2}$, σ_t) in the adjacent lamellar structures.

The NWZ structure of welded joint of pilot alloy 2, as in alloy 1, is characterized with formation of the extended lamellar type phases (α′-martensite and β-phase), but significantly different (approximately 2–3 times) in sizes, namely width of lamellar structures ($h_{lam} \sim 0.2–0.5$ μm), more disperse acicular α′-martensite structure and interlamellar substructure as well as more uniform distribution of dislocations ($\rho \sim (8–9) \cdot 10^{10}$ cm^{-2}) in all volume of the NWZ metal (Figure 10). There are differences in process of forma-

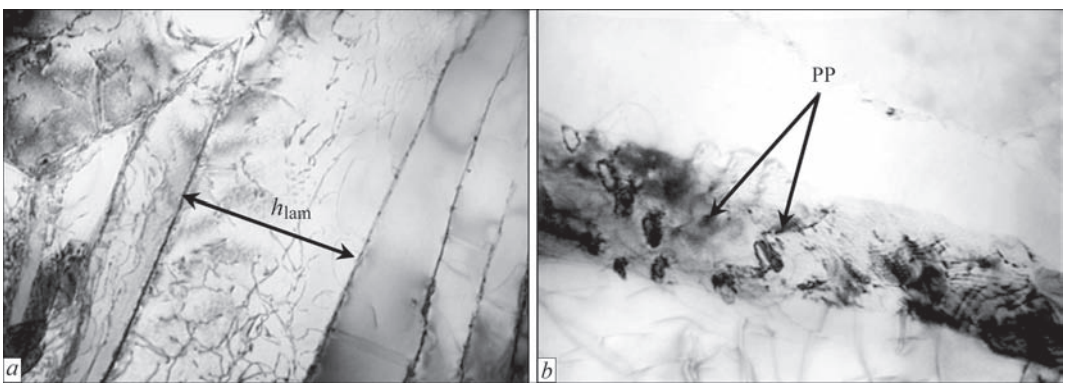

Figure 9. Microstructure (×20000) of pilot titanium alloy 1, NWZ: *a* — strictly oriented lamellas of mainly α-containing structure at comparatively low density and uniform dislocation distribution; *b* — phase formation in internal volumes of β-lamellar structures, ×37000

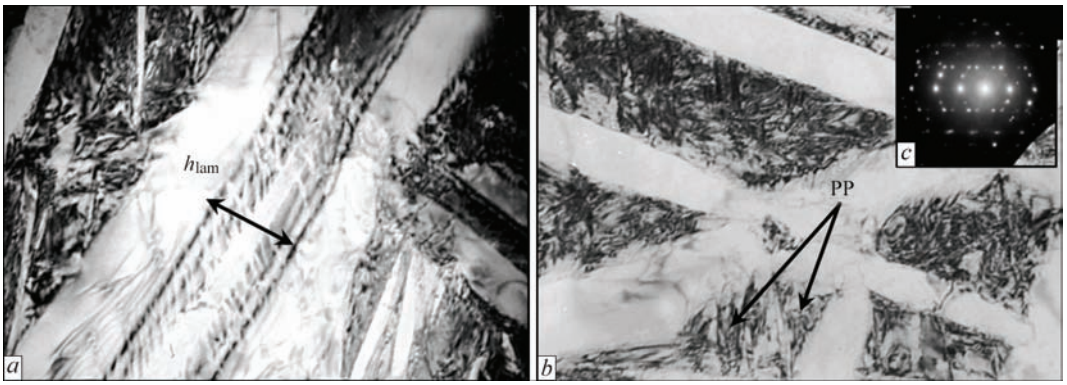

Figure 10. Microstructure of pilot titanium alloy 2, NWZ; *a*, *b* — fine structure of lamellar phases of martensite type (*a* — x50000; *b* — ×37000); *c* — microdiffraction reflections of PP, registered in combined images

tion of silicide intermetallic phases. At the same (as in the case of alloy 1) stoichiometric compostion (Ti_5Si_3; Ti_2ZrSi_3; Ti_3Al) phase sizes are more fine disperse (d_{pp} ~ 0.01–0.02×0.02–0.06 μm) and their distribution is uniform along the whole volume with localizing mainly on substructure boundaries (Figure 10, *b*).

The analytical evaluations of mechanical properties showed that HAZ metal of welded joints of pilot alloy 1 is characterized with strong gradient (approximately 1.8 times) change of yield strength ($\Delta\sigma_{0.2}$ ~ 570–1010 MPa), depending on structural-phase state of the lamellar structures (Figure 11). The rapid increase of $\Delta\sigma_{0.2}$, typical for the lamellar structures with high dislocation density ($\rho \sim (7–8)\cdot10^{10}$ cm^{-2}) and the most saturated phase precipitations, results in rise of dislocation ($\Delta\sigma_d$ ~ 250 MPa) and dispersion ($\Delta\sigma_{disp}$ ~ 375–500 MPa) hardening. The NWZ of alloy 2 has high level and more uniform distribution of strength characteristics ($\Delta\sigma_y$ ~ 910–1040 MPa) in forming martensite phases of lamellar type that is related with their more fine disperse structure. At that somewhat increase of hardening is caused by substructure dispersion ($\Delta\sigma_s$ ~ 530 MPa) and comparatively uniform rise of total dislocation density on metal volume results in hardening of around $\Delta\sigma_d$ ~ 360 MPa.

Thus, the analytical evaluations of differential input of different structural-phase factors and parameters, forming in the welded joints of investigated alloys, in change of mechanical characteristics ($\sigma_{0.2}$), showed that the NWZ of alloy 1 welded joints has significant change of σ_y in the adjacent lamellar structures from 570 MPa for lamellar α′-phase to low dislocation density to 1010 MPa for lamellas with high dislocation density and silicide precipitations. Alloy 2 NWZ has higher level and more uniform distribution of strength characteristics ($\sigma_{0.2}$ varies from 910 to 1040 MPa in all volume of the NWZ metal).

Local internal stresses in HAZ of pilot alloys welded joints were determined as a result of examination of the dislocation structure. It is shown that (Figure 12, *a*) HAZ metal of alloy 1 has strong gradient, directed along the lamellas, distribution of internal stresses (from 10–100 to 700–1100 MPa). It is related with change of dislocation density in the lamellas of different type: low ($\rho \sim (10^9–10^{10}$ cm^{-2}) and high ($\rho \sim (7–8)\cdot10^{10}$ cm^{-2}). However, there are areas with the higher local dislocation density ($\rho \sim 2\cdot10^{11}$ cm^{-2}), where local internal stresses $\tau_{l/in}$ reach 2000 MPa order. Alloy 2 HAZ is characterized with relatively uniform distribution of internal stresses ($\tau_{l/in}$ ~ 860–970 MPa) that corresponds to uniform dislocation density ($\rho \sim (8–9)\cdot10^{10}$ cm^{-2}) on interlamellar structures (Figure 12, *b*).

Thus, evaluations of changes of internal stresses τ_{in} in the NWZ of welded joints of investigated alloys, performed on the basis of examination of dislocation structures, showed that the NWZ of alloy 1 welded joints has a very nonuniform distribution of internal stresses (approximately 10 times gradient), and directed along the lamellar structures in the lamellas with low and high dislocation density. The NWZ of alloy 2 welded joints has a more uniform distribution of internal stresses, however, connection of direction of the distribution of local internal stresses and lamellar structures can be a reason for directed crack propagation. Therefore, in order to eliminate gradient on strength

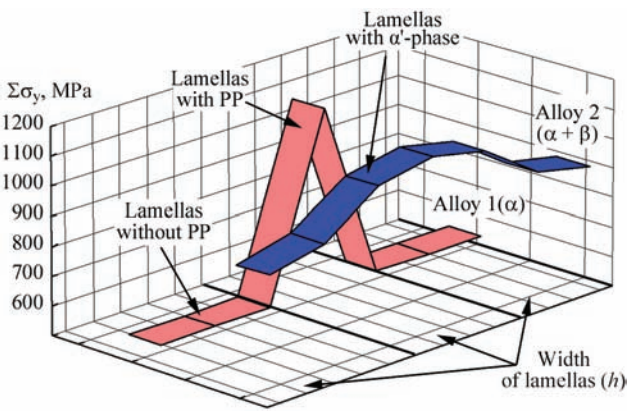

Figure 11. Input of different constituents of structural hardening (grain, subgrain, dislocation, dispersion) of pilot alloys in calculation value of hardening ($\Sigma\sigma_y$)

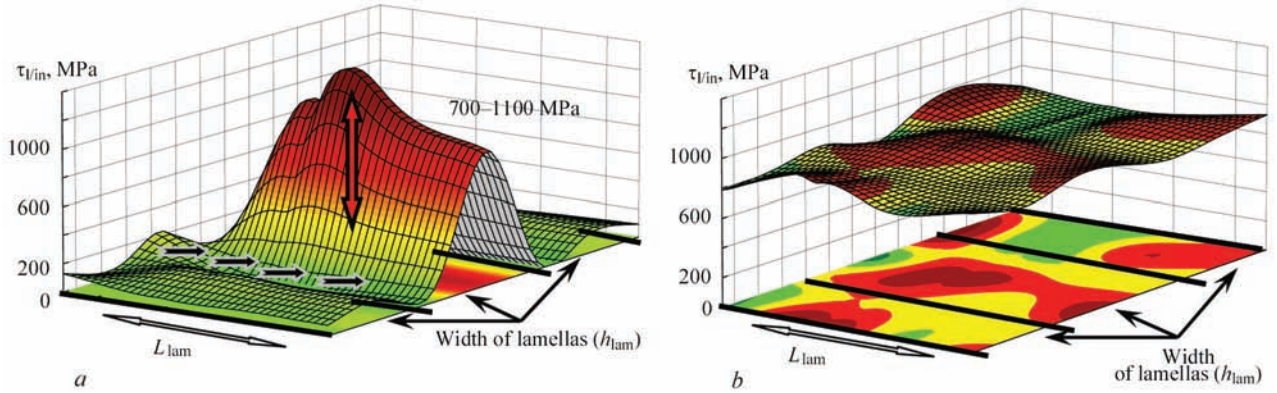

Figure 12. Level of local internal stresses forming in lamellar structures of NWZ of welded joints: *a* — in lamellar structures, gradient on distribution of dislocation density and intravolume PP (pilot alloy 1); *b* — in martensite lamellar structures (pilot alloy 2)

and internal stresses it is necessary to achieve formation of homogeneous uniform dispersed structure.

Conclusions

1. Complex investigations were carried out at all structural levels (from grain to dislocation) for study of structural-phase changes in metal of welded joints of high-strength steels, complexly-alloyed aluminium-lithium and titanium alloys, produced by different methods of welding (hybrid laser-arc welding, argon-arc welding, friction stir welding, electron beam welding).

2. Combination of examinations at different structural levels with analytical evaluations of mechanical properties in the produced welded joints determined interconnection of structural changes with variation of the most important for service conditions mechanical characteristics of the welded joints, namely indices of strength (σ_y), fracture toughness (K_{1c}) and crack resistance ($\tau_{l/in}$).

3. It is determined that the most optimum structural factors providing necessary complex of the welded joint properties under service conditions, namely properties of strength (σ_y), fracture toughness (K_{1c}) and crack resistance ($\tau_{l/in}$), are fine of grain and subgrain structures; dispersion of phase precipitations at their uniform distribution; absence of extended dislocation accumulations, i.e. potential concentrators of internal stress (zones of nucleation and propagation of cracks).

1. (1965) *High-strength steel*: Coll. Ed. by L.K. Gordienko. Moscow: Metallurgy.
2. Houdremont, E. (1959) *Special steels*. Moscow: Metallurgizdat.
3. Fridlyander, I.N. (2000) Aluminium alloys in aircrafts during 1970–1999 and 2000–2015. In: *Proc. of Sci. Council on New Materials of IAAS: Problems of Modern Materials Sciences*. Kiev: Naukova Dumka, 15–19.
4. Solonin, O.P., Glazunov, S.G. (1976) *Heat-resistant titanium alloys*. Moscow: Metallurgiya.
5. Chechulin, B.B., Ushkov, S.S., Razuvaeva, I.N. et al. (1977) *Titanium alloys in machine-building*. Moscow: Mashinostroenie.
6. Markashova, L.I., Poznyakov, V.D., Berdnikova, E.N. et al. (2016) Structure and service properties of hybrid laser-arc welded joints of 14KhGN2MDAFB steel. *The Paton Welding J.*, **5/6**, 104–113.
7. Markashova, L.I., Poklyatsky, A.G., Kushnaryova, O.S. (2016) Effect of structure and properties of aluminium-lithium alloy welded joints produced by argon-arc and friction stir welding methods. *Ibid*., 81–85.
8. Markashova, L.I., Akhonin, S.V., Grigorenko, G.M. et al. (2012) Structure and properties of welded joints on titanium alloys containing silicon additions. *Ibid*., **11**, 6–15.
9. Markashova, L.I., Poznyakov, V.D., Berdnikova, E.N. et al. (2014) Effect of structural factors on mechanical properties and crack resistance of welded joints of metals, alloys and composite materials. *Ibid*., **6/7**, 22–28.
10. Markashova, L., Kushnareva, O. (2014) Effect of structure on the mechanical properties of the metal of welded joints of aluminium alloys of the Al–Cu–Li system. *Mater. Sci*., 49(**5**), 681–687.
11. Goldshtejn, M.I., Litvinov, V.S., Bronfin, B.M. (1986) *Physics of metals of high-strength alloys*. Moscow: Metallurgiya.
12. Conrad, H. (1973) *Model of strain hardening for explanation of grain size effect on flow stress of metals. In: Superfine grain in metals*. Ed. by L.K. Gordienko. Moscow: Metallurgiya.
13. Armstrong, R.V. (1973) Strength properties of superfine grain metals. *Ibid*., 11–40.
14. Petch, N.J. (1953) The cleavage strength of polycrystalline. *J. Iron and Steel Inst*., **173**, 25–28.
15. Orowan, E. (1954) *Dislocation in metals*. New York: AIME.
16. Ashby, M.F. (1983) Mechanisms of deformation and fracture. *Adv. Appl. Mech*., **23**, 117–177.
17. Romaniv, O.N. (1979) *Fracture toughness of structural steels*. Moscow: Metallurgiya.
18. Stroh, A.N. (1954) The formation of cracks as a recoil of plastic flow. *Proc. of the Roy. Soc. A*, 223(1154), 404–415.
19. Panin, V.E.,Likhachev, V.A., Grinyaeva, Yu.V. (1985) *Structure levels of deformation of solids*. Siber. Depart.: Nauka.
20. Conrad, H. (1963) Effect of grain size on the lower yield and flow stress of iron and steel. *Acta Metallurgica*, **11**, 75–77.

Received 01.04.2017